

Europe's Lost Frontiers

General Editor
Vincent Gaffney

Volume 1

Context and Methodology

edited by
Vincent Gaffney and Simon Fitch



Europe's Lost Frontiers

Volume 1

Context and Methodology

edited by

Vincent Gaffney and Simon Fitch

general editor

Vincent Gaffney



ARCHAEOPRESS PUBLISHING LTD
Summertown Pavilion
18-24 Middle Way
Summertown
Oxford OX2 7LG

www.archaeopress.com

ISBN 978-1-80327-268-9
ISBN 978-1-80327-269-6 (e-Pdf)

© Archaeopress and the individual authors 2022

Cover: Eleanor Ramsey

This book is available in print and as a free download from www.archaeopress.com



This work is licensed under a Creative Commons
Attribution-NonCommercial-NoDerivatives 4.0 International Licence



Landing by Ava Grauls (Duncan of Jordanstone College of Art & Design).
Oil and watercolour on Japanese shōji (障子) paper. 413 x 244cm

Landing is about location, ownership, shifting land and shifting borders. The painting was conceived after talking to academics about the space between Britain and Europe, and asking the question: 'How do you paint a forgotten landscape?' Landing was made to travel and interact with different environments and can be folded up and packed away into four boxes.

Ava Grauls 11/08/2021

Dedicated to our Families
For putting up with Doggerland for longer than any families since the Mesolithic

Handwritten signature in black ink, appearing to read "V.L. Soffey".Handwritten signature in black ink, consisting of stylized initials.

November 2021

Europe's Lost Frontiers

Europe's Lost Frontiers was funded through a European Research Council Advanced Grant (project number 670518). The European Research Council's mission is to encourage the highest quality research in Europe through competitive funding and to support investigator-driven frontier research across all fields, on the basis of scientific excellence. The European Research Council complements other funding activities in Europe such as those of the national research funding agencies, and is a flagship component of Horizon Europe, the European Union's Research Framework Programme.



European Research Council

Established by the European Commission

Contents

List of Figures	iii
General Editor's Preface	vii
The Lost Frontiers Team	viii
Authors' details	ix
Acknowledgements	xi
Chapter 1 Europe's Lost Frontiers: context and development.....	1
Vincent Gaffney and Simon Fitch	
Before Europe's Lost Frontiers	
Chapter 2 Beyond the site: A re-evaluation of the value of extensive commercial datasets for palaeolandscape research.....	16
Simon Fitch and Eleanor Ramsey	
Chapter 3 A description of palaeolandscape features in the southern North Sea	36
Simon Fitch, Vincent Gaffney, Rachel Harding, James Walker, Richard Bates, Martin Bates and Andrew Fraser	
Chapter 4 From extensive to intensive: Moving into the Mesolithic landscape of Doggerland.....	55
Simon Fitch	
Chapter 5 The archaeological context of Doggerland during the final Palaeolithic and Mesolithic.....	63
James Walker, Vincent Gaffney, Simon Fitch, Rachel Harding, Andrew Fraser, Merle Muru and Martin Tingle	
Europe's Lost Frontiers	
Chapter 6 The Southern River: methods for the investigation of submerged palaeochannel systems	89
Simon Fitch, Richard Bates and Rachel Harding	
Chapter 7 Establishing a lithostratigraphic and palaeoenvironmental framework for the investigation of vibracores from the southern North Sea	100
Martin Bates, Ben Gearey, Tom Hill, David Smith, John Whittaker and Erin Kavanagh	
Chapter 8 Sedimentary ancient DNA palaeoenvironmental reconstruction in the North Sea landscape.....	112
Robin Allaby, Rebecca Cribdon, Rosie Everett and Roselyn Ware	
Chapter 9 Palaeomagnetic analysis of cores from Europe's Lost Frontiers.....	122
Samuel E. Harris, Catherine M. Batt and Elizabeth Topping	
Chapter 10 Applying chemostratigraphic techniques to shallow bore holes: Lessons and case studies from Europe's Lost Frontiers.	137
Alexander Finlay, Richard Bates, Mohammed Bensharada and Sarah Davies	
Chapter 11 Introduction to geochemical studies within Europe's Lost Frontiers	154
Mohammed Bensharada, Ben Stern and Richard Telford	

Chapter 12 Constructing sediment chronologies for Doggerland	165
Tim Kinnaird, Martin Bates, Rebecca Bateman and Aayush Srivastava	
Chapter 13 Building chronologies for Europe’s Lost Frontiers: Radiocarbon dating and age-depth modelling	181
Derek Hamilton and Tim Kinnaird	
Chapter 14 Simulating a drowned landscape: A four-dimensional approach to solving problems of behaviour and scale	190
Phil Murgatroyd, Eugene Ch’ng, Tabitha Kabora and Micheál Butler	
Chapter 15 Greetings from Doggerland? Future challenges for the targeted prospection of the southern North Sea palaeolandscape	208
Simon Fitch, Vince Gaffney, James Walker, Rachel Harding and Martin Tingle	
 Supplementary Data	
Chapter 16 Supplementary data to ‘The archaeological context of Doggerland during the Final Palaeolithic and Mesolithic’ by Walker, Gaffney, Fitch, Harding, Fraser, Muru and Tingle	217
James Walker, Vincent Gaffney, Simon Fitch, Rachel Harding, Andrew Fraser, Merle Muru and Martin Tingle	
Chapter 17 Supplementary data to ‘Constructing sediment chronologies for Doggerbank, North Sea’ by Kinnaird, Bates, Bateman and Srivastava	218
Tim Kinnaird, Martin Bates, Rebecca Bateman and Aayush Srivastava	
Bibliography	222

List of Figures

Frontispiece	Landing by Ava Grauls (Duncan of Jordanstone College of Art & Design)	
Figure 1.1	Survey areas prior to Europe’s Lost Frontiers discussed in this chapter. (1) North Sea Palaeolandscape Project (2) Humber REC (3-4) West Coast Palaeolandscape Project. ASTER DEM is a product of METI and NASA. ETOPO2v2 is the property of the National Geophysical Data Centre, NOAA, US Dept of Commerce.....	2
Figure 1.2	Area of Doggerland mapped by the North Sea Palaeolandscape Project (Gaffney <i>et al.</i> 2009: Figure 3.23).	3
Figure 1.3	Red flag mapping from Gaffney <i>et al.</i> (2007: Figure 9.8). This image combines threat and uncertainty data based on distance to feature and depth of overlying sediment. The lack of sediment cover and direct association with identified features with archaeological potential rate as high threats with little uncertainty. Deep overlying deposits lying farther from recorded features rank as low threat areas but with significant levels of uncertainty.....	4
Figure 1.4	Distribution of features located within the southern North Sea during the NSPP and BSSS projects.....	6
Figure 1.5	Map used in the final ERC application showing course of two submerged river valleys to be targeted for coring by the Lost Frontiers project team, overlaid on NSPP project base map (Gaffney <i>et al.</i> 2007).	8
Figure 1.6	Initial modification of the Europe’s Lost Frontiers coring programme following funding in 2016.....	10
Figure 1.7	Additional modifications to Europe’s Lost Frontiers coring programme following BREXIT.....	11
Figure 1.8	Final Europe’s Lost Frontiers coring programme.....	13
Figure 1.9	Europe’s Lost Frontiers core study area (1), Cardigan and Liverpool Bays (3) and area of study added as part of the Brown Bank survey (2).	14
Figure 1.10	Iterative research methodology within Europe’s Lost Frontiers.	15
Figure 2.1	Timeslice at 0.076s through the Southern North Sea MegaSurvey 3D seismic dataset. The NSPP study area is outlined in blue and the extended study area discussed within this paper is outlined in red.....	17
Figure 2.2	Graph of the frequency from the PGS MegaSurvey 3D seismic data.....	18
Figure 2.3	Additional, original 3D datasets utilised for comparison with data generated through MegaSurvey processing....	19
Figure 2.4	Data comparison for survey Z3NAM1988A.....	20
Figure 2.5	Frequency values within the 3D legacy seismic volumes assessed within this study.....	21
Figure 2.6	Frequency values within the Parametric Echo Sounder dataset.	22
Figure 2.7	Cross-checking between horizontal and vertical slices within the 3D dataset. (A) shows correlation across a wide area with multiple responses along highlighted line, whilst (B) shows the correlation across highlighted line for a single feature.....	4
Figure 2.8	Features within sample area, digitised within SMT Kingdom.....	25
Figure 2.9	Features identified within sample area, imported into an ArcGIS project.....	26
Figure 2.10	Features within the ArcGIS project cleaned and simplified.	26
Figure 2.11	A timeslice with opacity filters applied (B), whilst (A) is the resulting interpretation of features derived from image B. It is clear the combination of opacity filters on the timeslice supports fine resolution imaging of small-scale features within this river drainage.	27
Figure 2.12	An RMS slice from the Outer Silver Pit area. The slice is generated from the volume between 0s and 0.1s.	29
Figure 2.13	Base horizon layer imported from SMT Kingdom into GIS.....	30
Figure 2.14	Areas used to split the horizon point dataset.	30
Figure 2.15	Detail within Area 1, showing band divisions used to de-stripe the data.	31
Figure 2.16	Interpolated raster of Area 1 prior to manual de-stripping.....	31
Figure 2.17	Interpolated raster of Area 1 after manual de-stripping.....	32
Figure 2.18	3D vertical exaggeration of features within Area 1 using ArcScene.	32
Figure 2.19	Interpolated raster mosaic after values for Area 1 and Area 2 had been re-evaluated.....	33
Figure 2.20	A 3D Geobody Model, constructed from the seismic timeslices, and displayed within the seismic volume.....	34
Figure 2.21	A channel visualised by cutting the geobody model to reveal the base of the channel model. By using such methods, it is possible to understand, more fully, the morphology and formation of such structures.....	34
Figure 3.1	GIS Mapping of the features recorded by the Europe’s Lost Frontiers project.	37
Figure 3.2	Seismic line from ‘Gauss 159B’ survey acquired in 1990 by the RGD and BGS over the Dogger Bank. A Holocene channel can clearly be seen to be incised into the underlying late Pleistocene deposits (Dogger Bank Formation).	37
Figure 3.3	Areas divisions of landscape features within the study area.	38
Figure 3.4	Cross section across the southern flank of the Dogger Bank. The Holocene features can be seen to incise into the underlying late Pleistocene deposits.....	39
Figure 3.5	Example of the later Holocene reuse of pro-glacial channels. This is evidenced by smaller (black) channels cut within the main valley and the formation of dendritic feeders on the side of the valley.	40
Figure 3.6	The main drainage channels of the Dogger Bank drain south into a major channel located at the foot of the bank and in the area of the Oyster Ground, eventually flowing to the west and into the Outer Silver Pit.	41
Figure 3.7	Mottling of the seismic data within the Oyster ground can clearly be seen in this image. A number of small palaeochannels can also be seen through the mottling.....	42
Figure 3.8	Area 1, early Holocene features of the Dogger Bank. The main watersheds are shown as dashed black lines, the features in the southwest of Area 1, including the Shotton River, would have been the longest-lived structures on the Dogger Bank.....	43

Figure 3.9	Map of the Eastern Sector/Area 2.....	44
Figure 3.10	The extent of wetland response is outlined within the red hashed area. The location of BRITICE core 147VC is marked in orange.....	45
Figure 3.11	Interpretation of a seismic line crossing the base of the Dogger Bank area (near the area marked B in Figure 3.8) clearly shows a large channel running at the base of Dogger Bank (shown here as the DB5 unit between 141VC and 140VC) (Roberts <i>et al.</i> 2018: Figure 6).....	46
Figure 3.12	Cross section across the east of the Oyster ground. The topographic rise which forms the watershed is apparent.....	47
Figure 3.13	Location of mapped features within Area 3.	48
Figure 3.14	Topographic depressions southeast of the Outer Silver Pit (Area 3).....	49
Figure 3.15	Early Holocene landscape features in Area 4.	50
Figure 3.16	Mapped palaeochannels in Area 2 flow towards the -40m bathymetric contour, below this line virtually no features are mapped. This supports the hypothesis that the axial area was a marine inlet during the Holocene/Mesolithic.....	51
Figure 3.17	Major features, Late Palaeolithic c. 11,500 BP.	52
Figure 3.18	Coastlines of early Mesolithic Doggerland c. 10,000 BP.....	53
Figure 3.19	Coastlines of Mesolithic Doggerland c. 8500 BP.....	53
Figure 3.20	Coastlines of the earliest Neolithic c. 7000 BP.....	54
Figure 4.1	Location of the Arch-Area_1 study area is shown by a red box. Bathymetric data courtesy of EMODNET Bathymetry Portal, ETOPO1 topographic data courtesy of the NCEI and NOAA.....	56
Figure 4.2	The NSPP 2007 interpretation of the channel system overlain on EMODNET bathymetry.....	57
Figure 4.3	Multibeam Bathymetric image of the survey area generated through the Humber REC.....	58
Figure 4.4	Humber REC 2D seismic line over main channel and tributary channel.....	60
Figure 4.5	Humber REC 2D seismic line showing several strong reflectors in the main channel.....	60
Figure 4.6	A timeslice from the 3D seismic data at 0.076s derived from the PGS Megamerge dataset. The red box is the position of the Humber REC 2D survey, and the position of vibracores VC39/39A and VC40 are shown as yellow circles.	61
Figure 4.7	Comparison between the GIS channel outlines as derived from A) the Humber REC 2D survey interpretation and B) the NSPP survey GIS interpretation. Both are overlain on a depth surface derived from the Humber REC 2D dataset.....	61
Figure 5.1	A) The Colinda ‘harpoon’, found within a chunk of ‘moorlog’ peat dredged from the Leman / Ower banks off the Norfolk coast in 1931 (after Flemming 2002); B) A bone point recovered from beach walking at Massvlakte 2 in the Netherlands (courtesy of Luc Amkreutz); C) An array of barbed bone points from Maasvlakte 1 off the Dutch coast (courtesy of the Rijksmuseum van Oudheden). Many other examples of organic artefacts from Dutch waters may be found in Peeters and Amkreutz (2020), Amkreutz and Spithoven (2019) and Louwe Kooijmans (1970).....	65
Figure 5.2	Temperature curve for the Final Pleistocene and Early Holocene (Late Glacial and Postglacial between 17 and 7 thousand years ago) as derived from Greenland Ice Core data, and redrawn from Price (2015). Note the climatic variability of the Final Pleistocene relative to that of the Holocene.	66
Figure 5.3	Map showing the projected coastlines of Doggerland and the southern North Sea since the final millennia of the Last Glacial Maximum, with key dates for the transgression highlighted.	68
Figure 5.4	The sites and findspots located on the map are a combination of the SplashCOS viewer database, and data points presented in Tables (5.1 and 5.2), with the exception of findspots from Norwegian waters beyond the extent of the map. See this volume, chapter 16 for further information.....	71
Figure 5.5	Four snapshots of landscape evolution across the period of 10,000–7000 cal BP. The period in question spans both the 8.2 ka cold event, and the Storegga tsunami, and shows different stages of Doggerland as it transitioned into an archipelago and, eventually, a littoral fringe landscape.....	76
Figure 5.6	Anders Fischer’s model for the predictive location of submerged Mesolithic sites has been used to great effect in the nearshore waters in and around Denmark. Image from Fischer (2007). The model shows potentially favourable site locations in different coastal landscapes: A) near an estuary mouth or inlet with access to a hinterland; B) in close proximity to islands, but with preference for landward situation; C) on headlands, with particular preference for (D) those offering access to sheltered waters; and E) at river mouths, with preference for (F) flat and even ground.....	78
Figure 5.7	River Valleys active in the Mesolithic, identified through seismic survey and palaeobathymetry, and marked by blue arrows.....	80
Figure 5.8	The location of Core ELF001A where evidence of Storegga tsunami run-up deposits in highly localised areas prompted reconsideration of the event’s impact.....	86
Figure 6.1	The location of the Southern River is within the box on the main map.	91
Figure 6.2	The location of the 2D seismic data shown in Figures 6.3 and 6.4 is indicated by the black line (top). The lower image is an example of the original 2D Boomer dataset used for targeting the cores within the Southern River. ..	92
Figure 6.3	2D Boomer data after bandpass filtering applied.....	93
Figure 6.4	2D Boomer data after amplitude and gain correction applied.....	93
Figure 6.5	A combined Bathymetric and seismic data surface of the Southern River. The dendritic network is visible at the head of the river, whilst sinuosity increases as the river proceeds south towards the location of the Holocene coastline.	96
Figure 6.6	A seismic cross section showing the position of the Humber REC core Arch VC51 and Europe’s Lost Frontier’s cores ELF006 and ELF001A.....	97
Figure 6.7	The distinctive laminated sediments (SRF6) that produce a clear signal in the seismic data are visible in these images of cores ELF033 and ELF054.....	98

Figure 7.1	Distribution of cores taken during Europe's Lost Frontiers	100
Figure 7.2	Flow diagram illustrating pathways of samples in the laboratory.	102
Figure 7.3	Cold storage facility for the Lost Frontiers Project at Lampeter (Left). Core recording (Right).....	103
Figure 7.4	Cores ELF 47 and ELF 51.....	105
Figure 7.5	Basic lithological profiles drawn up in the Southern Valley.....	106
Figure 8.1	Differential sedaDNA fragmentation (top) and deamination (bottom) damage patterns in Doggerland palaeoenvironments. Fragmentation expressed as the lambda parameter of the exponential distribution of sedaDNA fragment sizes. Deamination expressed as the probability of observing a C to T change at the terminal position (position 0) of the 5' end of DNA fragments, caused by cytosine deamination.....	115
Figure 8.2	Coring sites used for sedaDNA analysis. A) Cores 1-20. B) Cores in range 21-60 over the Southern River area. C) Cores 20-60. D) Core sites selected for deep sequencing. Estimated 8200 BP coastline shown in black and estimated Storegga tsunami run up extent shown in white. The Storegga tsunami core (ELF001A) shown in grey.	120
Figure 9.1	Locations of cores used in this study.	122
Figure 9.2	Schematic representation of the detrital remanent magnetisation mechanism from left to right - how the acquisition of the geomagnetic field occurs in sediments.	123
Figure 9.3	Location of the UK archaeomagnetic PSVC (Meriden: 52.43°N, -1.62°E), UK Lake Windemere sequence WINPSV_12k (Avery <i>et al.</i> 2017), and FENNOSTACK comprised of seven lake sediment sequences from four lakes (Snowball <i>et al.</i> 2007).	124
Figure 9.4	Sampling of core ELF019 during the first sampling trip (© Erin Kavanagh).....	125
Figure 9.5	Palaeomagnetic analysis procedure followed when full analysis takes place.	127
Figure 9.6	Comparison of the Inclination data isolated through PCA with associated errors against the WINPSV-12k (Avery <i>et al.</i> 2017) calibration curve.	128
Figure 9.7	Left: Magnetic susceptibility values for core ELF001A averaged from three separate runs and corrected for drift of sensor. Features on the plot are noted in the text. Right: Image of the core for comparisons.	129
Figure 9.8	Stratigraphic trends of the rock magnetic parameters for ELF001A. The plots show the variations in a) magnetic susceptibility, b) susceptibility of ARM, c) S-ratio, d) Saturation Isothermal Remanent Magnetisation (SIRM), e) ARM _x /SIRM ratio, f) percentage of bIRM acquired between 0-20mT, and g) the Coercivity of Remanence.....	131
Figure 9.9	Left: Magnetic susceptibility values for core ELF002 averaged from three separate runs and corrected for drift sensor. Features on the plot are noted in the text. Right: Image of the core for comparisons.....	132
Figure 9.10	Left: Magnetic susceptibility values for core ELF003 averaged from three separate runs and corrected for drift sensor. Features on the plot are noted in the text. Right: Image of the core for comparisons.....	133
Figure 9.11	Left: Magnetic susceptibility values for core ELF019 averaged from three separate runs and corrected for drift sensor. Features on the plot are noted in the text. Right: Image of the core for comparisons.....	134
Figure 9.12	The declination and inclination values plotted down core for ELF019 from the analysis of 21 samples.....	135
Figure 9.13	Down core plot of magnetic proxies calculated for core ELF019.	135
Figure 10.1	A summary of the benefits of typical analytical tools utilised in chemostratigraphic studies and their acronyms.....	138
Figure 10.2	Location map of cores referred to in this paper. Bathymetric data is derived from the EMODnet Bathymetry portal - http://www.emodnet-bathymetry.eu . Topographic data derived from the NOAA ETOPO1 dataset, courtesy of the NCEI - https://www.ngdc.noaa.gov/mgg/global/	140
Figure 10.3	PCA of elemental data for core ELF19 showing the likely mineralogical and material drivers for variation in elemental compositions. a - component 1 and 2, b - component 2 and 3.....	141
Figure 10.4	Chemostratigraphic zonation of core ELF19. Si/Rb likely reflects variations in grain size with higher values being more Sand (Quartz) rich and higher Rb being more Clay rich. Ca/Rb likely reflects variations in carbonate (Ca) compared to clay material. S/Rb likely reflects variations in organic material (S) to clay. Br/Ti is a proxy for salinity in wetlands (see text for references).....	142
Figure 10.5	Boxplots showing the correlation of observed mineralogy and chemistry within core ELF19.	144
Figure 10.6	This figure demonstrates an excellent match in the chemostratigraphic zonation of core ELF19 and ecological biostratigraphic data.....	146
Figure 10.7	Orkney core locations	147
Figure 10.8	The elemental variations utilised to define the chemostratigraphic zonation in the study area. Sr/Br likely reflects variations in shell material (Sr - aragonite) and organic material (Br). Sr/Rb likely reflects variations in shell material (Sr - aragonite) and Clay (Rb). Si/Br likely reflects variations in sand (Si - Quartz) and organic material (Br).	148
Figure 10.9	Chemostratigraphic correlation of chemo zones in wells A, B and C.....	149
Figure 10.10	Chemostratigraphic correlation of chemo sub zones in wells A, B and C.	149
Figure 10.11	Chemostratigraphic zonation of core ELF1A (from Gaffney <i>et al.</i> 2020). Sr likely reflects the amount of shell material (aragonite) Rb likely reflects the amount of clay, Si likely reflects the amount of sand (Quartz) and Zr the amount of detrital zircon in the core.	150
Figure 10.12	Chemostratigraphic zonation of the Storegga tsunami deposit preserved in core ELF1A (from Gaffney <i>et al.</i> 2020).....	150
Figure 10.13	Comparison of the relative density of core ELF1A calculated from XRF data to the interpreted seismic data (from Gaffney <i>et al.</i> 2020).	152
Figure 11.1	Locations of the three cores mentioned in the text.....	155
Figure 11.2	Extracted ion chromatogram (EIC), for 71m/z showing n-alkanes in the sample ELF002.	157
Figure 11.3	Extracted ion chromatogram (EIC) for 71m/z, showing n-alkanes in the sample ELF007	157

Figure 11.4	Extracted ion chromatogram (EIC) for 71m/z, showing n-alkanes in the sample ELF009.	157
Figure 11.5	Fatty acids found in sample ELF002.	159
Figure 11.6	Fatty acids found in sample ELF007.	159
Figure 11.7	Fatty acids found in sample ELF009.	159
Figure 11.8	XRD pattern of sample ELF002.	160
Figure 11.9	XRD pattern of sample ELF007.	160
Figure 11.10	XRD pattern of sample ELF009.	160
Figure 11.11	Comparison between the ELF002 pattern and the standard of quartz, berlinite and calcite.	162
Figure 11.12	PXRD of ELF007 overlain with reference patterns of quartz, berlinite and halite.	163
Figure 11.13	PXRD of ELF009 overlain with reference patterns of quartz and halite.	163
Figure 12.1	Locations of cores mentioned in text.	166
Figure 12.2	For successful OSL dating, both environmental and mineral characteristics are important: zeroing during transport and deposition is a function of environmental conditions and luminescence behaviour.	167
Figure 12.3	Illustrative luminescence-depth plots for the Doggerland cores: illustrating, (A., ELF05B) stratigraphic breaks and temporal discontinuities, (B., ELF012) rapid sedimentation and short chronology, (C., ELF022) slow sedimentation and long chronology, (D., ELF051) stratigraphic breaks, stratigraphic progressions and cyclicity.	169
Figure 12.4	Sampling strategy for ELF cores – illustrated with core ELF001A: (a) core, with sub-units identified; (b) core, with sampling positions indicated; (c) removal of sediment for OSL profiling, OSL dating and dosimetry.	171
Figure 12.5	Illustrative luminescence-depth plots for ELF001A: on the left, IRSL and OSL net signal intensities and depletion indices; on the right, apparent dose and sensitivity distributions.	172
Figure 12.6	D _e distributions for ELF001A, 90-150µm, shown relative to the stratigraphy of the core. Units for ELF001A as discussed in the text.	177
Figure 12.7	Stored dose estimates for the 90-150µm and 150-250µm quartz fractions.	178
Figure 12.8	Dosimetry of core ELF001A: semi-quantitative and absolute down-core variations in radionuclide concentrations.	179
Figure 12.9	(left) Apparent vs stored dose estimates for discrete depths in core across a subset of sampled cores, encompassing terrestrial, littoral and marine deposits; (right) Quartz SAR OSL depositional ages shown relative to depth in core for the same subset of cores.	180
Figure 13.1	Locations of cores mentioned in this chapter.	183
Figure 13.2	Age-depth model for ELF001A. Each distribution represents the relative probability that an event occurred at some particular time. For each OSL measurement two distributions have been plotted, one in outline, which is the original result, and a solid one, which is based on the chronological model use. The other distributions correspond to aspects of the model. For example, 'start: Unit 5' is the estimated date that this litho-stratigraphic change occurred, based on the dating results. The large square 'brackets' along with the OxCal keywords define the overall model exactly.	184
Figure 13.3	Age-depth model for ELF007. The model is described in Figure 13.2, with the exception that the outline of the radiocarbon dates is based on the simple calibration of those measurements, whereas the solid ones are the result of the modelling.	186
Figure 13.4	Age-depth model for ELF034. The model is as described in Figures 13.2 and 13.3.	187
Figure 13.5	Calibrated humin fraction and humic acid pairs for depths 180, 185, 193, 202, and 209cm in core ELF034.	188
Figure 13.6	Detail of the bottom of the age-depth model for ELF034. In this detail the humin fraction and humic acid dates at each level have been plotted side-by-side, rather than combined as in Fig 13.4, to show the relationship of each result to the conservative model results for the bottom of the core.	189
Figure 14.1	The simulation conceptual framework.	196
Figure 14.2	3D visualisation package, showing part of the Southern River valley terrain with simulated sea level.	197
Figure 14.3	A 3D render of the output of the forest dynamic modelling package.	198
Figure 14.4	Graphical output from the landscape modelling package showing areas with differing amounts of inundation over time.	198
Figure 14.5	A screenshot of the quadtree-based large-scale modelling infrastructure, showing herbivore agents responding to resources in a landscape. The red squares show the dynamic partitioning of the environment resulting from the quadtree structure.	199
Figure 14.6	The ELF Augmented Reality sandbox.	200
Figure 14.7	The ELF Augmented Reality sandbox in use.	200
Figure 14.8	The Model 1.1 simulation study area.	201
Figure 14.9	Relative sea-level change over the last 21,000 years in the North Sea region from Glacial Isostatic Adjustment (GIA) model reconstructions (Bradley <i>et al.</i> 2011; Shennan, Bradley and Edwards 2018).	203
Figure 14.10	Table of data showing headings.	204
Figure 14.11	Graph showing one calendar year's data of water height and atmospheric pressure effect.	204
Figure 14.12	Graph showing 14 year's water height data.	205
Figure 14.13	Flowchart of the Europe's Lost Frontier models.	206
Figure 15.1	Areas designated for windfarm development within UK and Belgian waters and survey lines associated with the Brown Bank and Southern River study areas (The Crown Estate ©, bathymetry derived from EMODNET. Topography derived from ETOPO)	209
Figure 15.2	Survey on the Southern River estuary	211
Figure 15.3	A flint hammerstone fragment, approximately 50mm wide, was retrieved during a 2019 survey of the Southern River valley (offshore north of the Norfolk coast) from (or near) a surface dated to 8827±30 cal BP SUERC-85715 (Missiaen <i>et al.</i> 2021). Scanned image courtesy of Tom Sparrow.	213
Figure 17.1	Equivalent dose distributions for units 4, 5, 6 and 7 from ELF001A as histogram plots	221

List of Tables

Table 1.1	Numbers and area of features, excluding coastlines, identified through the NSPP and BSSS projects (2008-2012). After Gaffney <i>et al.</i> 2011: Table 5.1	7
Table 2.1	Additional, original 3D datasets used for cross comparison purposes.	19
Table 5.1	Mesolithic sites and findspots from territorial waters, the nearshore zone (<12 nautical miles of the shoreline) of the North Sea basin. This table excludes submerged sites and findspots located from inland waters (rivers, inlets and estuaries) in Essex (UK) and the Limfjord (Denmark). For category Type: CF = Collection of Finds; SF = Single Find; (U) = Unstratified; (S) = Stratified. For category Dating: C14 = Radiocarbon Dating; T-C = Typo-chronology; Strat = Stratigraphically; SLC = Sea Level Curve. For Sources, BMAPA stands for British Marine Aggregate Producers Association. Age estimates are given in approximate years BC, and depth is given in metres. Some locales comprise multiple findspots, and grid references are approximate. Data primarily compiled using SplashCOS Viewer available at www.SplashCOS.maris2.nl	70
Table 5.2	Palaeolithic, Mesolithic and Neolithic findspots from the offshore zone beyond territorial waters (>12 nautical miles of the shoreline) of the North Sea basin. For category Type: CF = Collection of Finds; SF = Single Find; (U) = Unstratified; (S) = Stratified. For category Dating: C14 = Radiocarbon Dating; T-C = Typo-chronology; Strat = Stratigraphically. For category Sources: RMO stands for Rijksmuseum van Oudheden. Age estimates are given in approximate years BC, and depth is given in metres. Some locales comprise multiple findspots, and grid references are approximate. Data primarily compiled (excluding the Southern River find) using SplashCOS Viewer available at www.SplashCOS.maris2.nl	70
Table 6.1	Geological deposits within the study area.....	90
Table 6.2	Seismic facies within the Southern River system	99
Table 7.1	ELF 045, lithology table.....	104
Table 7.2	Cores sampled in project. Abbreviations as follows: P1, profile 1, uncalibrated OSL; P2, profile 2, calibrated OSL; D, OSL sediment ages.....	108
Table 7.3	Example of data from rapid assessment of cores samples.....	109
Table 7.4	Detailed assessment of microfossils from ELF 047.	110
Table 7.5	Cores selected for pollen and diatom investigation.	111
Table 7.6	Cores samples for macrofossil analysis.....	111
Table 9.1	Summary of palaeomagnetic sampling details with core locations.....	126
Table 9.2	The stage of palaeomagnetic analysis carried out on each core to date: X denotes completion, P denotes partial analysis. Magnetic susceptibility carried out on obtained samples at the University of Bradford (1) and carried out using the handheld MS2K directly on the core sections (2).....	127
Table 9.3	Definitions of magnetic proxies referred to in text and used to characterise the magnetic minerals present.....	130
Table 10.1	Elements commonly utilised for archaeological and paleoenvironmental research (summarised from Davies <i>et al.</i> 2015 and Chemostrat multiclient report NE118).....	139
Table 10.2	Likely elemental affinities for core ELF19.	142
Table 10.3	Chemical definition of Chemo Zones and boundaries for core ELF19.	143
Table 10.4	Integrated chemical and ecological results for core ELF19.	145
Table 10.5	Chemical, sedimentological and environmental interpretation of chemo zones and integrated facies identification.....	148
Table 10.6	Chemo facies identified in core ELF1A (see Gaffney <i>et al.</i> 2020 supplementary information for full discussion). ..	151
Table 10.7	A summary interpretation of geochemical and seismic datasets.....	153
Table 11.1	Core identifiers, location and depth.....	155
Table 11.2	The percentage of organics and carbonates.	156
Table 11.3	Characteristic (2 θ) values, and the d-spaces of standards and the obtained samples pattern.	161
Table 12.1	Stored dose estimates for the 90-150 μ m quartz fractions from ELF001A (lab code, CERSA114).	178
Table 12.2	Weighted combinations of OSL depositional ages for ELF001A.	179
Table 17.1	Observations / inferences from preliminary OSL screening and subsequent calibrated OSL characterisation, example ELF001A.....	219

The Lost Frontiers Team

University of Bradford

Dr Andrew Fraser
Dr Ben Stern
Dr Catherine Batt
Dr James Walker
Dr Philip Murgatroyd
Dr Rachel Harding
Dr Richard Telford
Dr Simon Fitch
Dr Tabitha Kabora
Micheál Butler
Mohammed Bensharada
Professor Vincent Gaffney
Sam Harris
Dr Helen McCrearey
Elizabeth Topping
Anne Harvey
Tim Squire-Watt

University of Aberystwyth

Professor Sarah Davies

University of Bath

Dr Matt Law

University of Birmingham

Dr David Smith
Eamonn Baldwin

Chemostrat

Dr Alexander Finlay

University College Cork

Dr Ben Gearey
Dr Kevin Kearney

Flanders Marine Institute

Dr Tine Missiaen
Dr Ruth Plets

National University of Ireland, Galway

Eoghan Daly

University of Glasgow

Dr Derek Hamilton

INFOMAR

Kevin Sheehan

Natural History Museum

Dr John Whittaker

University of Nottingham, Ningbo

Professor Eugene Ch'ng

PalaeoEnvironmental Research and Consultancy Services Ltd

Dr Tom Hill

Sligo Institute of Technology

Dr James Bonsall
Eithne Davis

University of Wales, Trinity St Davids

Dr Martin Bates
Erin Kavanagh

University of St Andrews

Professor Richard Bates
Dr Tim Kinnaird
Rebecca Bateman
Aayush Srivastava

University of Tartu

Dr Merle Muru
Dr Alar Rosentau

University of Warwick

Dr Rebecca Cribdon
Dr Roselyn Ware
Professor Robin Allaby
Dr Rosie Everett

Wolverhampton and Walsall Historic Environment Record

Eleanor Ramsey

Dr Martin Tingle
Dr Wendy Carruthers

Authors' details

Robin Allaby, School of Life Sciences, Gibbet Hill Campus, University of Warwick, Coventry CV4 7AL, United Kingdom

Rebecca Bateman, School of Earth and Environmental Sciences, University of St Andrews, Bute Building, Queen's Terrace, St Andrews KY16 9TS, United Kingdom

Martin Bates, Faculty of Humanities and Performing Arts, University of Wales Trinity Saint David, Lampeter, Ceredigion SA48 7ED, United Kingdom

Richard Bates, School of Earth and Environmental Sciences, University of St Andrews, Bute Building, Queen's Terrace, St Andrews KY16 9TS, United Kingdom

Catherine M. Batt, School of Archaeological and Forensic Sciences, University of Bradford, Richmond Road, Bradford BD7 1DP, United Kingdom

Mohammed Bensharada, School of Archaeological and Forensic Sciences, University of Bradford, Richmond Road, Bradford BD7 1DP, United Kingdom

Micheál Butler, School of Archaeological and Forensic Sciences, University of Bradford, Richmond Road, Bradford BD7 1DP, United Kingdom

Eugene Ch'ng, NVIDIA Technology Centre, University of Nottingham Ningbo China, 199 Taikang East Road, Ningbo 315100, China

Rebecca Cribdon, School of Life Sciences, Gibbet Hill Campus, University of Warwick, Coventry CV4 7AL, United Kingdom

Sarah Davies, School of Geography and Earth Sciences, Llandinam Building, Penglais Campus, Aberystwyth University, Aberystwyth SY23 3DB, United Kingdom.

Rosie Everett, School of Life Sciences, Gibbet Hill Campus, University of Warwick, Coventry CV4 7AL, United Kingdom

Alexander Finlay, Chemostrat Ltd., 1 Ravenscroft Court, Buttington Cross Enterprise Park, Welshpool, Powys SY21 8SL, United Kingdom

Simon Fitch, School of Archaeological and Forensic Sciences, University of Bradford, Richmond Road, Bradford BD7 1DP, United Kingdom

Andrew Fraser, School of Archaeological and Forensic Sciences, University of Bradford, Richmond Road, Bradford BD7 1DP, United Kingdom

Vincent Gaffney, School of Archaeological and Forensic Sciences, University of Bradford, Richmond Road, Bradford BD7 1DP, United Kingdom

Ben Gearey, Department of Archaeology, Connolly Building, Dyke Parade, University College, Cork, Cork City T12 CY82, Ireland

Derek Hamilton, Scottish Universities Environmental Research Centre, Rankine Avenue, Scottish Enterprise Technology Park, East Kilbride G75 0QF, United Kingdom

Rachel Harding, School of Archaeological and Forensic Sciences, University of Bradford, Richmond Road, Bradford BD7 1DP, United Kingdom

Samuel E. Harris, School of Archaeological and Forensic Sciences, University of Bradford, Richmond Road, Bradford BD7 1DP, United Kingdom

Tom Hill, PalaeoEnvironmental Research and Consultancy Service, 67 Eastfield Road, Princes Risborough, Buckinghamshire HP27 0HZ / Department of Earth Sciences, The Natural History Museum, Cromwell Road, London SW7 5BD, United Kingdom.

Tabitha Kabora, Leverhulme Centre for Anthropocene Biodiversity, University of York, York YO10 5DD, United Kingdom

Erin Kavanagh, Arts Building, University of Birmingham, Edgbaston, Birmingham B15 2TT, United Kingdom

Tim Kinnaird, School of Earth and Environmental Sciences, University of St Andrews, Bute Building, Queen's Terrace, St Andrews KY16 9TS UK

Philip Murgatroyd, School of Archaeological and Forensic Sciences, University of Bradford, Richmond Road, Bradford BD7 1DP, United Kingdom

Merle Muru, Department of Geography, University of Tartu, 46 Vanemuise Str, 51003 Tartu, Estonia

Eleanor Ramsey, Wolverhampton and Walsall Historic Environment Record, Wolverhampton City Council, Civic Centre, St Peter's Square, Wolverhampton, WV1 1RP, United Kingdom.

David Smith, Classics, ancient History and Archaeology, University of Birmingham, Edgbaston, Birmingham B15 2TT, United Kingdom

Aayush Srivastava, School of Earth and Environmental Sciences, University of St Andrews, Bute Building, Queen's Terrace, St Andrew, KY16 9TS, United Kingdom.

Ben Stern, School of Archaeological and Forensic Sciences, University of Bradford, Richmond Road, Bradford BD7 1DP, United Kingdom

Richard Telford, Centre for Chemical and Biological Analysis, University of Bradford, Richmond Road, Bradford BD7 1DP, United Kingdom

Martin Tingle, 106 Brook Street, Wymeswold LE12 6TU, United Kingdom

Elizabeth Topping, School of Archaeological and Forensic Sciences, University of Bradford, Richmond Road, Bradford BD7 1DP, United Kingdom

James Walker [Archaeological Museum](#), University of Stavanger, 4036 Stavanger, P.O. box 8600, Norway

Roselyn Ware, School of Life Sciences, Gibbet Hill Campus, University of Warwick. Coventry CV4 7AL, United Kingdom

John Whittaker, Department of Earth Sciences, The Natural History Museum, Cromwell Road, London SW7 5BD, United Kingdom.

Chapter 6

The Southern River: methods for the investigation of submerged palaeochannel systems

Simon Fitch, Richard Bates and Rachel Harding

Introduction

The *Humber Regional Environmental Characterisation* (Humber REC) project (Tappin *et al.* 2011) identified an area in the southern North Sea that potentially preserved a late Mesolithic/early Neolithic landscape. The landscape contains river systems that were finally submerged at c. 6500 (\pm 500) BP (Tappin *et al.* 2011: 215). This result appeared to contradict dates provided by previous GIA modelling for the area (e.g. Shennan 2000), which suggested the area had been inundated by this date. The Humber REC therefore revealed the possibility of the existence of a tract of land extending from the north shore of East Anglia that was exposed during the Late Mesolithic to Early Neolithic. The existence of a Neolithic Doggerland is rarely considered although, Bryony Coles (1999) did discuss the possibility. Following analysis of seismic data acquired by industry and the Humber REC, the area, now known as the Southern River, was subject to a detailed coring program. Cores were located along the length of the palaeoriver channel on the basis that the temporal sequence of the transect might provide detailed information on the timing, progress and eventual submergence of the river. The Southern River Valley is not only a key area within the *Europe's Lost Frontiers* research programme, it provides an exemplar of the analysis of individual large channels within the project, and this chapter provides a preliminary description of methods and results of the seismic analysis in this valley.

Background geology of the Southern River Valley

The basement for this region consists of upper Palaeozoic through Mesozoic sediments including chalk, sandstone and siltstones. Regional structural patterns have been published in a number of oil and gas basin atlases, see for example Campbell (2013) and Cameron *et al.* (1992). These features provide the backbone of the landscape on which the overlying, more recent sediments are located. However, it is with the overlying, largely unconsolidated or partially consolidated geology that this study is mostly concerned.

During the Pleistocene, subsidence in the southern North Sea followed regional, underlying faulting

patterns with an approximately northerly trend. The subsidence occurred at a rate of approximately 0.5m per thousand year (Stoker *et al.* 1985). During the Early Pleistocene (2.5 Ma to 774,000 BP), deposits in the area are derived from a series of deltaic deposits which Long *et al.* (1988) observed to be both thick and laterally extensive. The provision of sediment from the British Isles into this depositional system is related to restricted deposits in the region, but the overall deposition reflects the dominant European input of sediment which extended the Netherlands delta plain (Zagwijn 1989). This massive input of material caused rapid sedimentation in the Southern Bight, which conversely starved the northern sector of the North Sea of sediment (Cameron *et al.* 1992).

The Middle Pleistocene (774,000 to 125,000 BP) begins with the record of glacial ice extending into the southern North Sea. Large 'scaphiform' tunnel valleys were created at the base of the ice sheet (Ehlers *et al.* 1984), and were subsequently infilled with glacial clay and later by lacustrine and marine clays. The glacial material in this region likely was deposited predominantly during the Anglian glaciation (Gibbard *et al.* 1991), which also caused the eventual blocking of the Southern Bight, thus diverting fluvial activity, including glacial melt water, south through the English Channel (Gibbard *et al.* 1988; Hamblin *et al.* 1992).

The late Pleistocene (125,000 to 11,650 BP) within the southern North Sea basin contains several glacial and interglacial periods (Laraminie 1989b) characterized by transitions between glacial, terrestrial and marine environments. The end of the period is marked by glaciolacustrine and glaciomarine infill. These geographical changes ultimately created the landscape to the extent that it can be traced today (Eisma, 1979). Whilst these terminal glacial deposits form the backbone of the recent geology within this region, later Holocene erosion and deposition has also been significant.

Holocene sediments dating from between 11,650 to 6500 BP, attain a thickness of 1 to 5m within the region, and locally, deposits can reach thicknesses of between 16 to 30m (Laraminie 1989a, Fitch *et al.* 2005). These

Geological Period	Archaeological Period	Date	Deposits
Mid to Late Holocene	Submerged	7,000BP to Present Day	Nieuw Zeeland Gronden Formation, Well Hole Formation, Modern Sediments
Early Holocene	Late Upper Palaeolithic/Mesolithic	11,500BP to 7,000BP	Nieuwkoop Formation, Naaldwijk Formation (previously Elbow Formation)
Earliest Holocene/ Late Pleistocene	Late Upper Palaeolithic	20,000BP to 11,000BP	Botney Cut Formation
Late Pleistocene	Upper Palaeolithic/ Late Middle Palaeolithic	50,000BP to 16,000BP	Well Ground Formation, Bolders Bank Formation
Middle Pleistocene	Lower Palaeolithic	420,000BP to 375,000BP	Egmond Ground Formation
Middle Pleistocene	Lower Palaeolithic	420,000BP to ?	Sand Hole Formation
Middle Pleistocene	Lower Palaeolithic	475,000 to 420,000BP	Swarte Bank Formation
Early Middle Pleistocene	Lower Palaeolithic	700,000 to 475,000BP	Yarmouth Roads Formation
Mesozoic	N/A	+60,000,000BP	Upper Cretaceous Chalk

Table 6.1 Geological deposits within the study area

Holocene deposits record the history of the emergent landscape and its subsequent marine transgression and are of central interest to archaeologists and the *Europe's Lost Frontiers* project. The Holocene sequence is divided into two formations, namely the Nieuwkoop, which consists of a freshwater peat and the Naaldwijk, which records tidal flats and salt marsh environments (Rijsdijk *et al.* 2005). These have previously been described as the Elbow Formation (e.g. Cameron *et al.* 1992) but are now recognised as separate entities. Overlying these deposits are modern marine sediments including extensive sand banks of the Nieuw Zeeland Gronden member (Table 1 & Cameron *et al.* 1992).

Sturt *et al.* (2013) provide models of marine inundation across the southern North Sea which show that the inundation had started in this area at c. 10,000 BP. The models demonstrate that marine inundation continued across the area until fully flooded at c. 7000 BP.

The study area

The 'Southern River' is located approximately 22km offshore from the coast of East Anglia (Figure 6.1). The river channel runs for almost 260km², with a mean water depth of 21m and localised deeps to -39m. The river feature has a bathymetric expression on the seafloor and thus has not been completely infilled. The origin of the channel follows a glacial meltwater outwash system, with the first part cut into the underlying deposits during the earlier Late Devensian (Dove *et al.* 2017). The Holocene aspect of this channel is extant through its re-use of this pre-existing channel, which is made visible via the later networks of sub-aerial feeder channels which must have formed between the late Pleistocene to early Holocene. The floodplain of the river is approximately 1.1km wide with an average channel width of c. 250m. The Holocene channel shows a typical river profile with two tributaries in the upper reaches and some additional minor dendric

tributaries joining these. The river channel would have experienced several periods of infilling, including fluvial sedimentation, estuarine deposition during inundation and eventually marine sedimentation following inundation. Given the regional history of infilling, it was speculated that evidence of the marine transgression might be preserved and that a coring programme along the length of the channel might capture the sequential history of infilling.

The presence of Holocene deposits in this area were first indicated following recovery of peat within a gravity core taken by the BGS (then known as the Institute of Geological Sciences) in the 1970s. This core recovered a peat which was covered by a series of Holocene laminated silts and clays of intertidal origin (Cook 1991). This core was re-evaluated by the Humber REC project (Gearey *et al.* 2017) which showed the presence of fluvial material of a Holocene date. Further cores, acquired nearby in 2008 by the Humber REC project, revealed that the area contains a variety of terrestrial, estuarine and fluvial deposits as well as associated peat material. The cores, dated between 9000 to 8000 BP (Tappin *et al.* 2011: 197), suggested that conditions might be good for preservation of environmental deposits, although the Humber REC remit did not allow for an evaluation of the wider landscape and environment in this area. However, this material was sufficient to suggest that features in this area may contain *in-situ* sediments of early Holocene age (Tappin *et al.* 2011: 225) that would support the academic aims of *Europe's Lost Frontiers*. Recently, nearby commercial development has revealed a similar Holocene environment on the Dungeon Wind Farm, c. 10km away from the study area (Brown *et al.* 2018). Here freshwater deposits have been dated at 9755 ±52 BP (UBA-33301) with a thin upper peat covered by a shelly sand potentially representing final submergence dated at 8411-8331 cal BP (GU-34111).

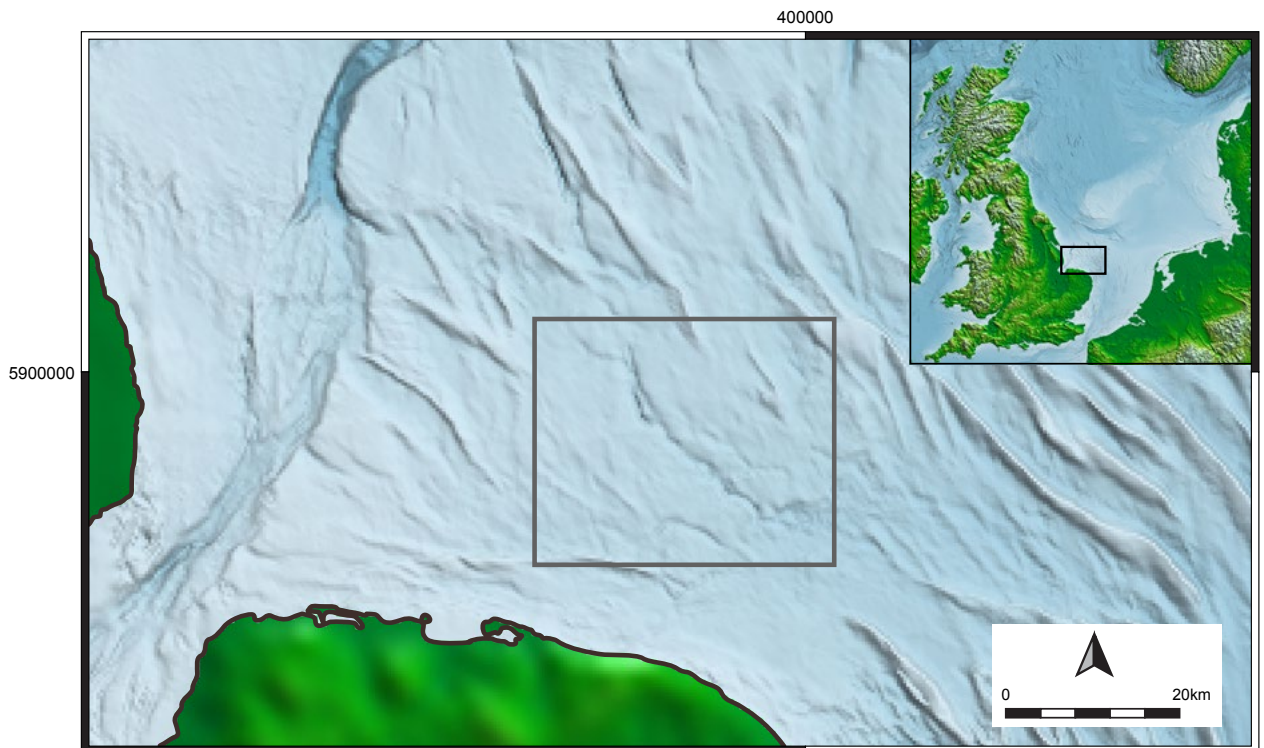


Figure 6.1 The location of the Southern River is within the box on the main map.

Methodology

An initial examination of the river channel was undertaken using bathymetric data from EMODNET. (<https://www.emodnet-bathymetry.eu/>). This data layer has a resolution of 115m and is suitable for displaying larger features which have a seabed expression. The bathymetric data indicates that the channel has a northwest-southeast orientation draining to the south and into a Holocene marine embayment (Figure 6.5).

Seismic interpretation of the data

The legacy seismic data available for this analysis was acquired by Gardline Surveys Ltd, using the vessel *Vigilant* equipped with a surface-towed boomer system (see Tappin *et al.* 2011: 73 for more details). This boomer system consisted of an Applied Acoustics 300 Plate powered by an Applied Acoustics CSP 1500 Pulse Generator and 12-element single channel hydrophone stream. The system was operated at a power level of 300 joules with a 350-millisecond fire rate. Initial data inspection and preliminary processing was accomplished using Chesapeake SonarWiz and Coda GeoSurvey (Figure 6.2). Processing included swell filtering, where necessary, and application of a band pass filter between 1kHz and 8.4kHz (Figure 6.3). All data was reduced to the Lowest Astronomical Tide Datum using predicted tidal ranges from the nearest

standard ports of Immingham and Cromer. Further processing utilising IHS Kingdom 2019 software was undertaken and included using a built-in running-sum amplitude gain correction filter (Figure 6.4).

Initial examination of the data showed a number of different seismic characters that were divided into seven distinct seismic facies. The seismic facies, prefixed 'SRF' (Southern River Facies), were determined using the seismic attributes of amplitude, frequency and continuity. Additional features of interest that were mapped included major reflection terminations (e.g. erosional truncations).

Targeted vibracoring

The *Europe's Lost Frontiers* vibrocores were acquired by Gardline, based on the project's interpretation of legacy seismic data. A total of 35 cores were acquired in this paper's study area, with a maximum penetration of 6m. Whilst it was noted that the 6m length of the available corer would not allow penetration of the deepest/oldest parts of the channel feature, the use of a longer corer would have been cost prohibitive and reduced the number of cores that could be acquired. In most cases the cores that were recovered were sufficient to support the project's goal of studying the early Holocene sequence. Core treatment followed the method outlined in Bates *et al.* (this volume).

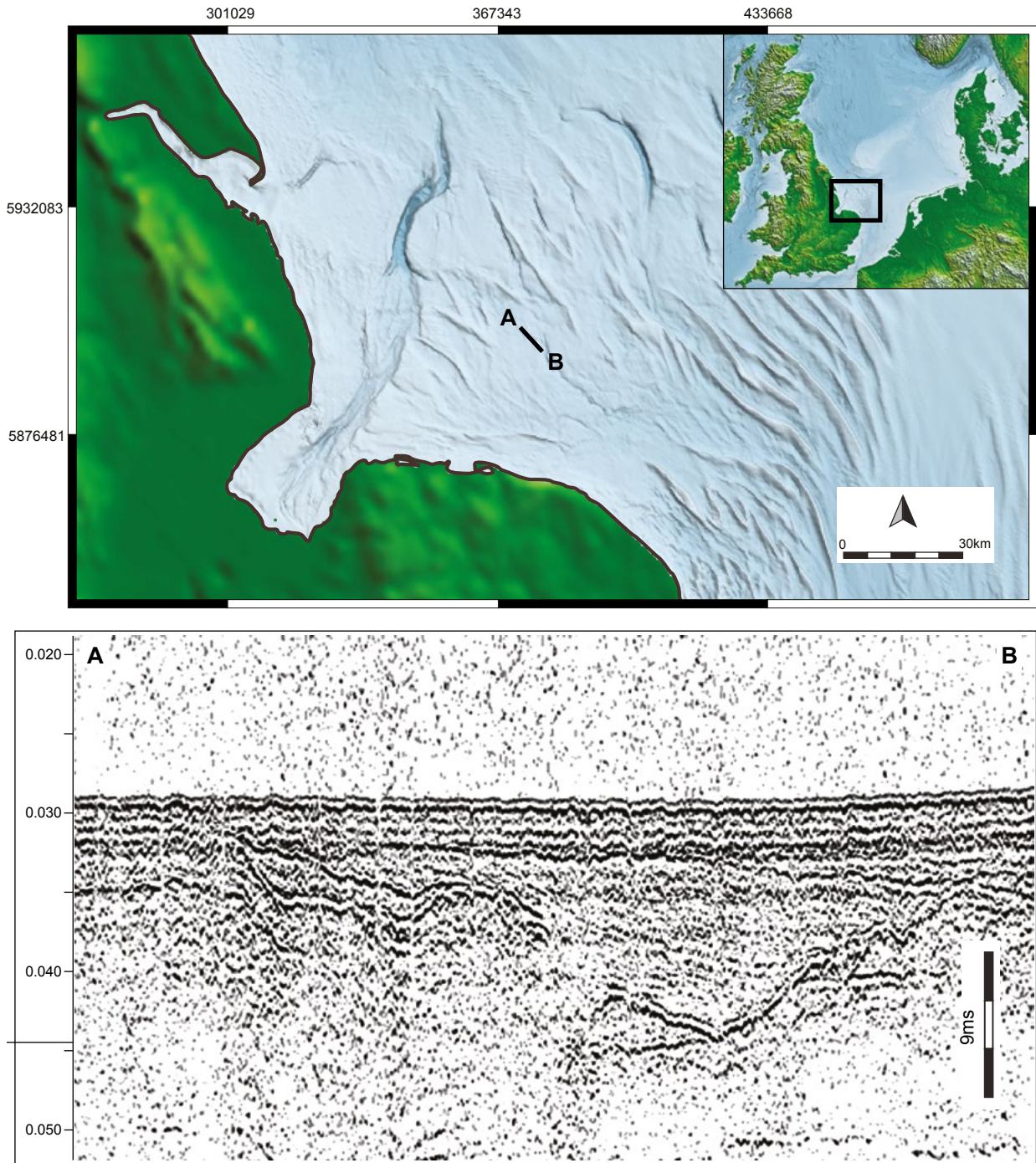


Figure 6.2 The location of the 2D seismic data shown in Figures 6.3 and 6.4 is indicated by the black line (top). The lower image is an example of the original 2D Boomer dataset used for targeting the cores within the Southern River.

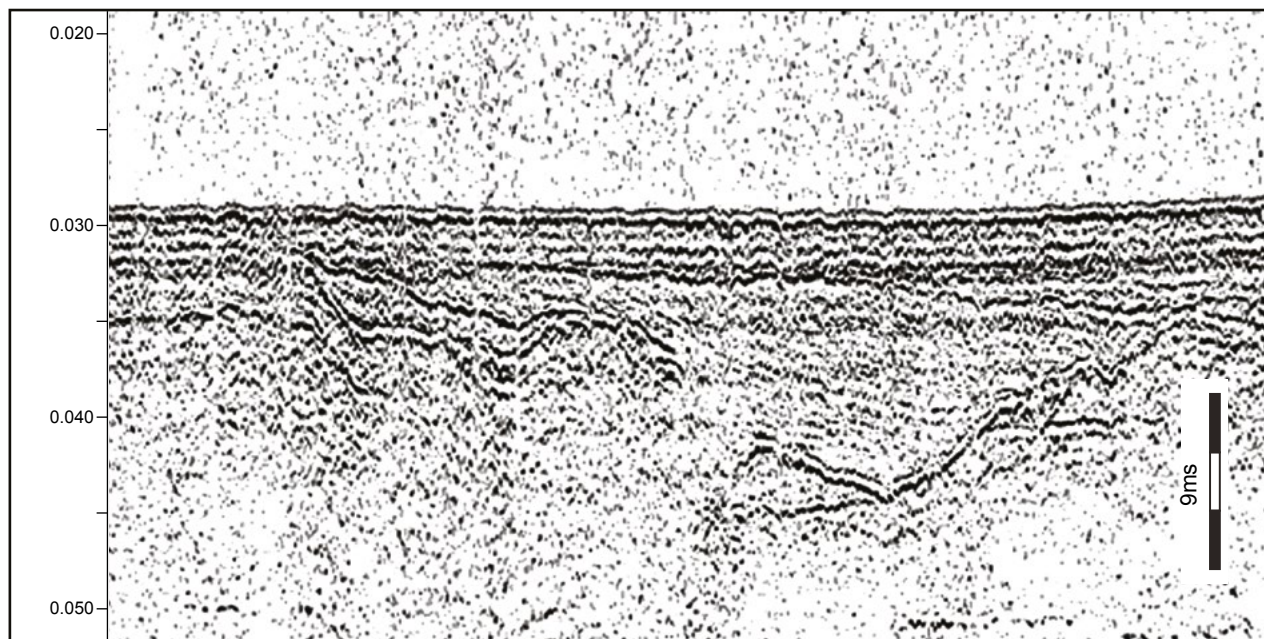


Figure 6.3 2D Boomer data after bandpass filtering applied.

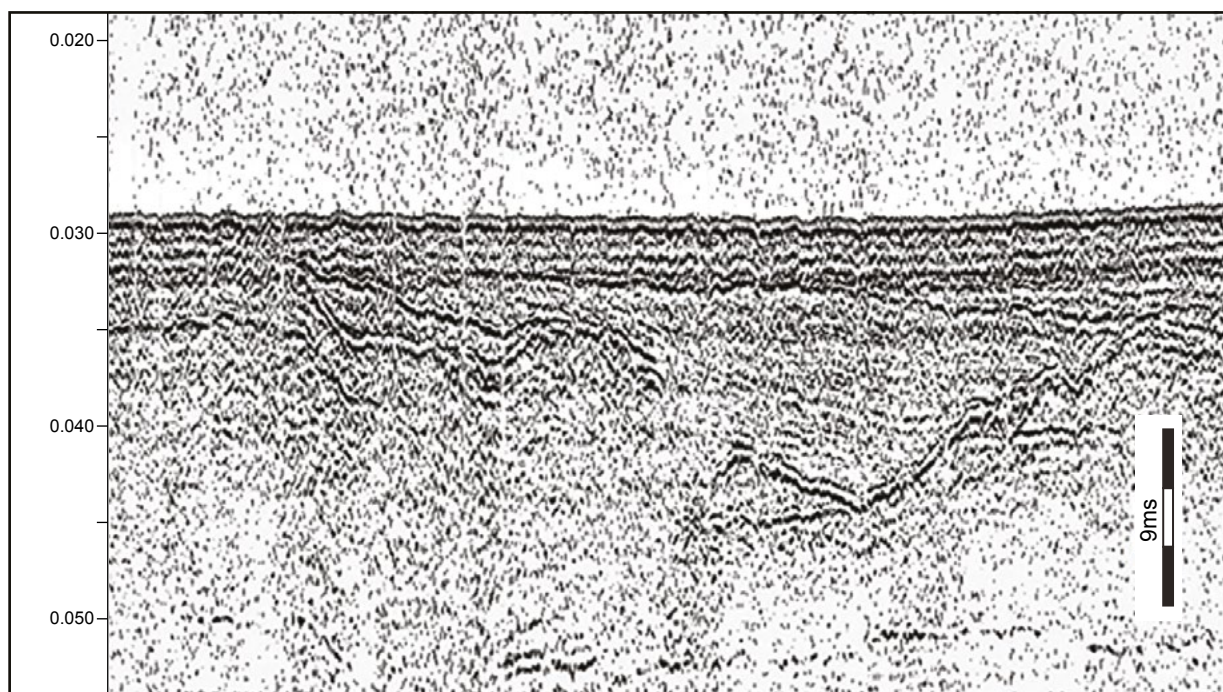


Figure 6.4 2D Boomer data after amplitude and gain correction applied.

Results: seismic facies

The seismic sequences of interest in Table 6.2 are described from the base of the sequence to the surface as seen in both the legacy industry 2D seismic and Humber REC seismic data. Data quality in the seismic dataset is highly variable due to differences in age (legacy data) and the inclement weather conditions during acquisition and the strength of seabed reflection (Humber REC). Boomer data was seen to have the best results in this area, and whilst maximum penetration depth of 50m was seen, the features were best resolved in the top 15m of the data.

SRF1

This is the deepest observable seismic facies in the boomer data and thus represents the seismic 'basement' for this study. The facies is characterised by having few internal reflections that are of high amplitude and low frequency. The internal reflections rarely extend laterally with opaque intervals of hundreds of metres. The unit is bound on its upper surface by a strong, regionally laterally continuous positive reflector.

SRF2

This is a geographically limited facies, being constrained to a small tunnel valley in the middle of the study area (Dove *et al.* 2017). The unit is moderately chaotic but has some internal discontinuous reflections that are of high amplitude and frequency. The unit fills the valley with an erosional truncation at its base that cuts into the SRF1 unit (Boundary SRB1). The unit is discordantly overlain by SRF6.

SRF3

This unit is geographically limited to both sides of the channel area. The facies is characterised by parallel internal reflection structures which are continuous within the unit. These parallel reflections are largely horizontal to sub-horizontal with a dip not exceeding 5 degrees and are of alternating high/low amplitude. The base of the unit is defined by an erosional truncation and can be seen to overlie SRF1. The unit is also overlain unconformably by SRF7

SRF4

This facies shows a massively chaotic internal reflection character with discontinuous internal reflections of high amplitude. The facies is bound by clearly definable high amplitude, high frequency boundaries. The deposits are cleanly cut into facies SRF1 and are separated by the erosional boundary SRB2. The SRF4 facies is overlain concordantly by SRF6 (Holocene age).

SRF5

This facies shows little structure with few, moderate amplitude internal reflectors. The facies is bound by clear channel cut reflectors at the base of a high amplitude, low frequency character. The base of SRF5 cuts down into the SRF1 deposits and is separated by the erosional boundary SRB3. Similar to other units in this area, the top of the facies is unconformably overlain by SRF6. Some opacity is seen in places, and this may relate to gas charging of the material.

SRF6

This unit is characterised by continuous, high amplitude internal parallel reflectors that are laterally continuous over tens of meters within the channel. The parallel reflectors are largely horizontal within the main body of the channel, but dip upwards to 30 degree with onlap at the channel margins. The base of the facies can be seen to unconformably overlie SRF2, SRF4 and SRF5 and is separated at the base by an erosional unconformity (SRB4) with high seismic amplitude.

SRF7

The top surface of this facies is represented by a high frequency parallel reflector which can be seen overlying all deposits in this region. The internal reflections are chaotic in nature and the facies has some localised variations in thickness. This material is separated at the base from the other facies by an erosional boundary SRB4 which is of a high amplitude nature.

Erosional boundaries

SRB1

This erosional boundary is demonstrated by the erosional truncation made into SRF1 deposits. The truncation is U shaped in form, and the boundary is of very high amplitude, moderate frequency and located at 0.066s in the seismic section.

SRB2

These boundaries are channel shaped with an irregular base, represented in the seismic data with a boundary of high frequency and a moderate amplitude. It is most closely associated with an irregular surface which is present between 0.062s and 0.050s in the seismic data.

SRB3

This erosional boundary is located between 0.053s to 0.037s. It is an irregular feature located above the SRB2 boundary and can be seen to separate SRF1 and

SRF5. The boundary is moderate frequency and high amplitude in nature.

SRB4

This is the latest erosional boundary in the seismic section. The boundary is located at 0.035s and 0.027s in the section. The boundary features high amplitudes and is of a moderately high frequency.

Discussion

New seismic reflection data has been divided into distinct units based on internal facies character and bounding contacts. Four major erosional boundaries (SRB1 to SRB4) have been identified that are consistently mapped across the survey area. The facies character and truncations can be interpreted to provide a sedimentological history consistent with the known regional patterns of geomorphological change during the Holocene.

The first phase of evolution mapped by seismics in this area, and the deepest recorded, starts with the formation of a glacial tunnel valley. Dove *et al.* (2017) suggest that the tunnel valleys likely correlate to the final position of ice in this area. This hypothesis finds support in recent investigations by Roberts *et al.* (2018). The base facies in this study (SRF1) shows identical acoustic characteristics to facies DB4 from Roberts *et al.* (2018: 193). Roberts correlates this material on the basis of cores taken by the BRITICE project to the Bolders Bank Formation, which is a sub glacial till located in complex sheet structures (Davies *et al.* 2011). The Bolders Bank formation was formed during the final major advance of the ice sheets and relates to ice front movements between 30,000 BP and 22,000 BP (Roberts *et al.* 2018). The SRF1 facies is cut into by the erosional boundary SRB1, whose character and overall shape match that for a typical glacial tunnel valley in the southern North Sea, and relates to glacial outwash.

Facies unit SRF2 partially fills the tunnel valley with onlap to the sides and an internal character that shows laterally discontinuous, bifurcating reflections. This character is consistent with an infilling of a channel by a fluvial system that is meandering across the accommodation space as a braided river system. An acoustic facies, DB5 was observed by the BRITICE project (Roberts *et al.* 2018), which possesses similar characteristics. The material was ascribed to the Botney Cut Formation, and Cotterill *et al.* (2017) suggests that the material may be related to pro-glacial drainage. The source of water for this fluvial activity was the outflow from glaciers to the north of region. The cold climate of the pro-glacial tundra provided ideal conditions for the formation of braided channels (Cotterill *et al.* 2017). The material SRF2 is thought to date to before the onset of

aridity due to the periglacial climate in the area (from c. 23,000 BP, Emery 2021: 118), and therefore of late Devensian age.

Following this arid stage there is a further period of late Pleistocene fluvial activity. The phase of activity is closely associated with an irregular surface present between 0.072s and 0.050s in the seismic data, which represents the channel cuts. The material contained within these channels (SRF4) appears to be associated with channel migration features, and gravel bottoms which show as a strong chaotic signal at the base of the features within the seismic data. These channels overlie or crosscut previous material and thus are later than 23,000 BP. Unfortunately, it is not possible to correlate these channels to previous studies, but it is possible that comparable features were observed by the BRITICE survey (Roberts *et al.* 2018) near the Southern River. These (DB5 and SRF2) were ascribed to the late Pleistocene/early Holocene Botney Cut Formation. It is known that a period of channel incision occurred elsewhere in the North Sea during the period 17,000 to 12,000 BP (Emery 2020). Given the channel stratigraphy seen in the seismic data, it is thought that the SRF4 deposits are related to this latest Devensian age (17,000 to 12,000 BP). OSL dates from ELF cores into these features have confirmed this association (see Kinnaird *et al.* this volume and forthcoming *Europe's Lost Frontiers* volumes for more details).

The third phase of fluvial activity relates to a reuse of earlier features and the full development of Holocene fluvial landscape through erosion and reuse of late Devensian structures (SRF3 & SRF5). The erosional boundary formed by this activity, SRB3, is located between 0.053s to 0.037s within the seismic data. These channels are smaller in size and form part of a sinuous dendritic river network that is visible within both the seismic data and bathymetry (Figure 6.5). The increase in sinuosity is thought to reflect the increased precipitation in the area and a warming climate. The smaller grain size of the material suggested in the seismic response of SRF5, reflects low sediment supply and source material from within the region. Similar channels were observed during the Humber REC and these were ascribed as Holocene fluvial systems (Tappin *et al.* 2011: 214). *Europe's Lost Frontiers* project cores which penetrated these deposits returned a similar Holocene age and thus the facies seen are thought to be identical to those observed by Tappin *et al.* 2011 (Figure 6.6). As these cores penetrate features that are broadly of similar morphology and age, and that are in close proximity (within 5km) to each other, it is reasonable to assume the sediments they contain are from the same unit.

The final phase relates to the development of estuarine deposits in the channels formed in response to sea-level rise in the early Holocene. These highly distinctive

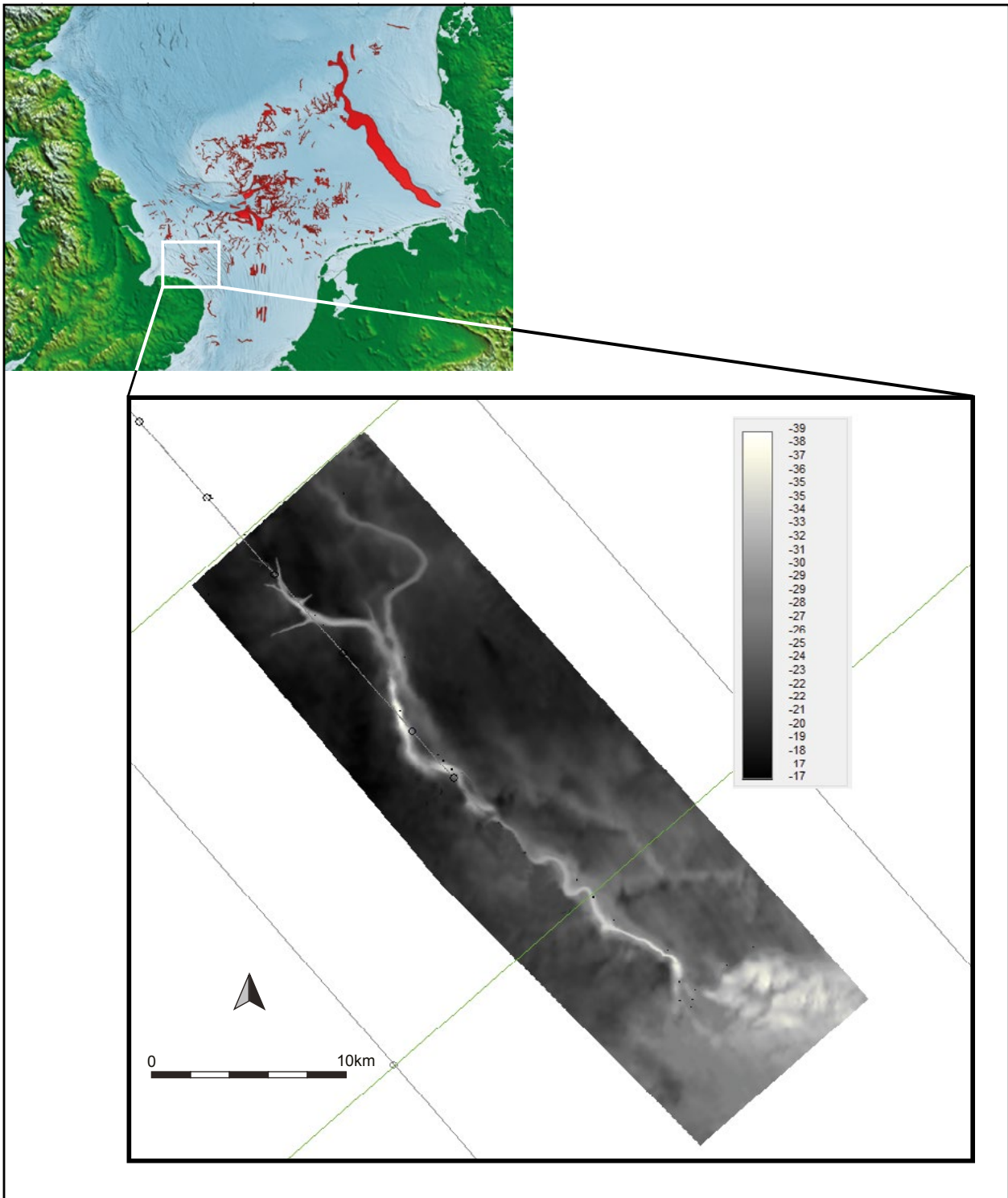


Figure 6.5 A combined Bathymetric and seismic data surface of the Southern River. The dendritic network is visible at the head of the river, whilst sinuosity increases as the river proceeds south towards the location of the Holocene coastline.

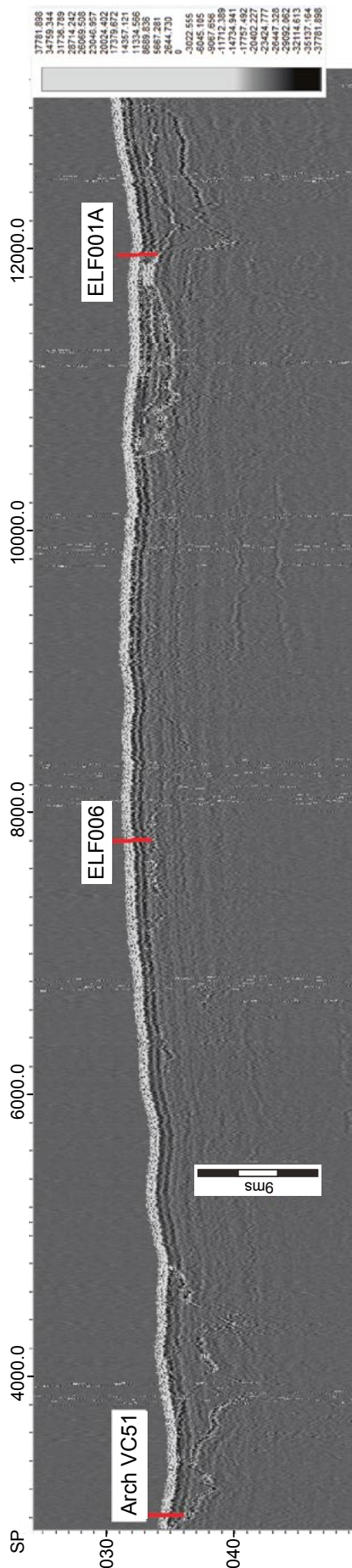


Figure 6.6 A seismic cross section showing the position of the Humber REC core Arch VC51 and Europe's Lost Frontier's cores ELF0006 and ELF001A.

laminated features (SRF6) are clearly visible in both the seismic data and core material recovered by *Europe's Lost Frontiers* (e.g. ELF054 and ELF033, Figure 6.7). Located between 0.035s and 0.027s, these reflect the tidal erosion surface (SRB4), and the later infilling of this and earlier landscape features, with intertidal silts and muds by SRF6. This sequence can be seen, repeatedly, in many *Europe's Lost Frontiers* cores along the southern river (see Bates *et al.* this volume and forthcoming *Europe's Lost Frontiers* volumes), and similar deposits were recovered during the Humber REC (Tappin *et al.* 2011: 194). The Humber REC also recovered cores from the SRF6 facies which comprised intertidal laminated silts and clays which dated to the period 9000 to 8000 BP (Tappin *et al.* 2011: 198). This material is therefore related to the final submergence of the Holocene landscape during the period 8500 to 8000 BP suggested by sea-level models (Shennan *et al.* 2000). It is, however, important to note that the Holocene channel cuts are in some parts of the study area not totally filled by this tidal silt and clay. This partial infilling, coupled with some modern erosion, has meant that some Holocene channel features have a reduced, but observable bathymetric expression on the current seabed.

The final facies within the dataset relates to modern sands (SRF7) which can be seen to overlay the entire study area and have been formed by more modern marine processes post 7000 BP.

Conclusions

The analysis presented here provides an example of the interpretative process carried out by *Europe's Lost Frontiers* researchers with respect of one, important feature. The data indicates that the channel system under study clearly has its origin in the advance and retreat of the ice sheet (Dove *et al.* 2017; Emery *et al.* 2019; Roberts *et al.* 2018). The channels cut the Bolders Bank formation till which, as observed by Roberts *et al.* (2018), is 'a series of overlapping sheets' relating to numerous ice front movements between 30,000 BP and 22,000 BP. Despite this, by c. 23,000 BP the ice sheets had advanced and retreated for the final time and the boulder clay and tunnel valley were subaerially exposed. The meltwater from the retreating ice then flowed, initiating the formation of the valley which constrained the later Southern River channel.

The interpretation of the seismic data therefore suggests that there are three distinct phases of channel development present:

1. an initial phase of incision by fluvio-glacial channels (Late Devensian – prior to 23,000 BP)
2. a later reuse and new channel formation stage (Late Devensian – 17,000 to 12,000 BP)

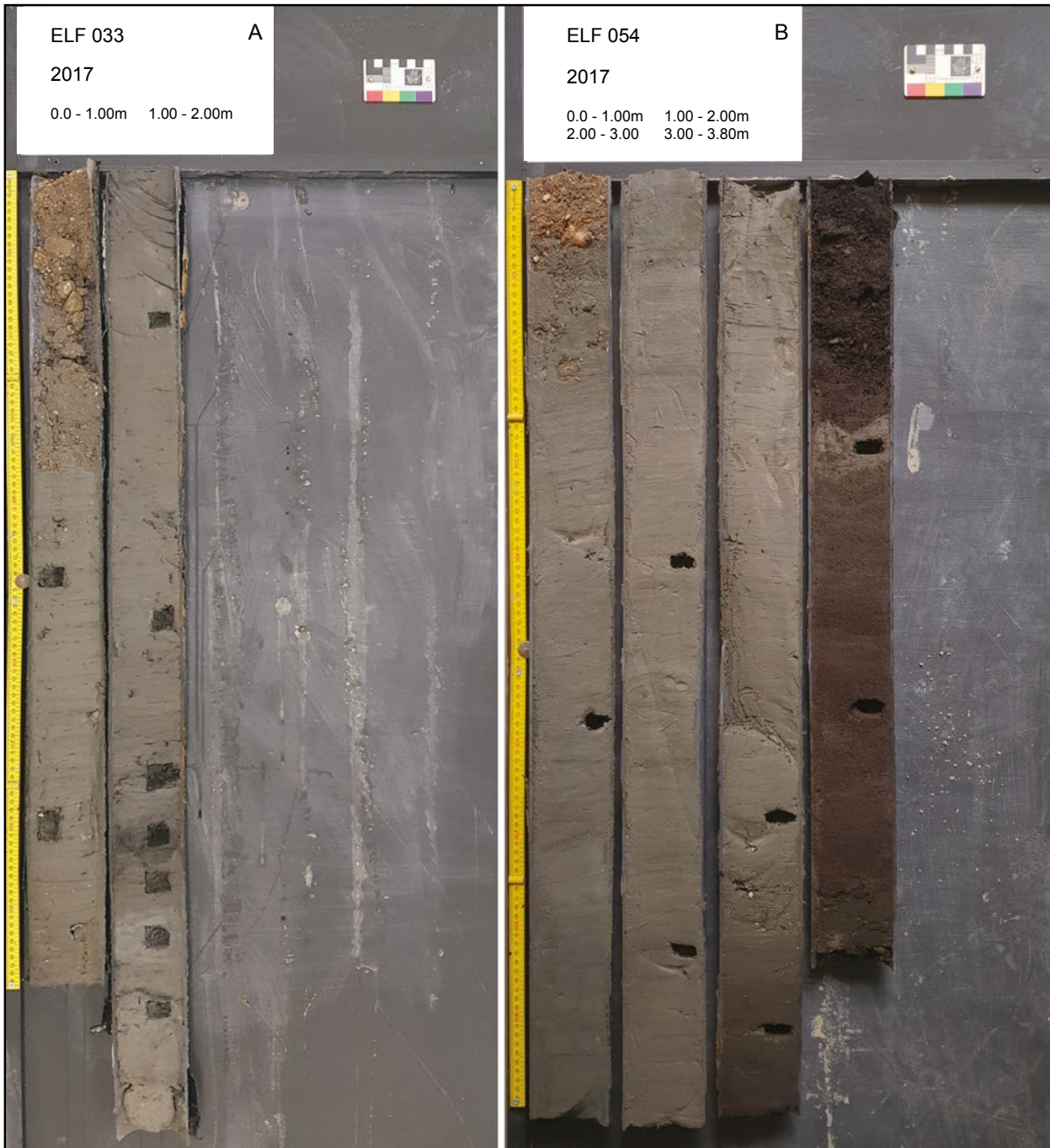


Figure 6.7 The distinctive laminated sediments (SRF6) that produce a clear signal in the seismic data are visible in these images of cores ELF033 and ELF054.

3. the final channel development (latest Pleistocene to early Holocene – 12,000 to 8000 BP)

The seismic data for this channel therefore records a history of landscape development after the ice. The data demonstrates not only the early phases of fluvial development, but also the responses of fluvial systems

and the landscape to sea-level rise and eventual submergence over an entire catchment. A full history of this channel, including a detailed geomorphological and environmental assessment, based on the new surveys, the core transect, as well as the archaeological context will be presented in later *Europe's Lost Frontiers* volumes.





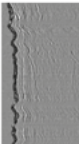





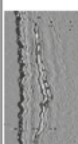

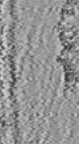
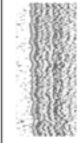
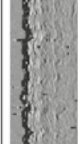

ELF Seismic Facies	ELF Example	ELF Character	ELF Reflector Configuration	ELF Interpretation	Tappin et al. 2011 (Humber REC)	Tappin 2011 Interpretation	Roberts et al. 2018	Roberts 2018 Units
SRF1 Chaotic Background		Variable frequency, low continuity	Chaotic bound by truncation above.	Boulder Clay from the Last Glacial Maximum		Boulders Bank Formation		DB4 Boulders Bank Formation, Boulder Clay
SRF2 Tunnel Valley Infill		High Amplitude, High Frequency, Moderate internal continuity	Moderately chaotic with some internal parallel reflectors. Cut into SRF1 deposits.	Late Devensian Tunnel Valley infilled with contemporaneous Fluvio-glacial deposits.		Late Glacial valley infill		DB5 Botney Cut Formation
SRF3 Holocene Floodplain		High Amplitude, medium frequency, high continuity	Agrading, Parallel, Largely conformable, with a very strong amplitude reflector at base found near to SRF8 and SRF7	Floodplain deposits - most likely silts and clays, moving into tidal flat deposits. Roberts et al. 2018 sampled the associated terrestrial peats with C14 dates ranging from 9.9 to 9.7 Ka BP		Holocene Sediments	UNRESOLVED	Unassigned - although peat units from this area ascribed to DB6 (Holocene)
SRF4 Chaotic Channel Infill		Variable frequency/low internal continuity	Highly Chaotic mass, bound by base channel reflector. Cut into SRF1 deposits	Latest Glacial/Earliest Holocene Fluvial Deposits - most likely sands and gravels	UNRESOLVED	Unassigned	UNRESOLVED	Unassigned - although may relate in part to DB5
SRF5 Holocene Channel Infill		High Amplitude, low frequency, low internal continuity	Small number of reflectors, bound by base channel reflector. Cut into SRF1 deposits. Opacity seen in some channels	Early Holocene Fluvial deposits. Opacity most likely caused by channel sands filled with gas		Holocene Sediments	UNRESOLVED	Unassigned
SRF6 Laminated Channel Infill		High Amplitude, medium frequency, high continuity	Agrading to Parallel with base usually cut into SRF1 deposits. Often overlies SRF6 and/or SRF7 deposits.	Laminated Silt and clays associated with muddy tidal flats and estuarine activity		Holocene Sediments	UNRESOLVED	Unassigned - although note in some cores laminated units below peat beds assigned to DB6 (Holocene)
SRF7 Modern Drape		Low Amplitude, high frequency, continuous across dataset	Agrading, Parallel.	Seafloor, with shallow modern sands		Modern Seabed Sands		DB7 Holocene Seabed sediments

Table 6.2 Seismic facies within the Southern River system